New scheme for the running coupling constant in gauge theories using Wilson loops

Erek Bilgici,[1,*] Antonino Flachi,[2,†] Etsuko Itou,[3,‡] Masafumi Kurachi,[4,§] C.-J. David Lin,[5,6,‖] Hideo Matsufuru,[7,¶] Hiroshi Ohki,[2,8,**] Tetsuya Onogi,[2,††] and Takeshi Yamazaki[9,‡‡]

[1]*Institut für Physik, Universität Graz, A-8010 Graz, Austria*
[2]*Yukawa Institute for Theoretical Physics, Kyoto University, Kyoto 606-8502, Japan*
[3]*Academic Support Center, Kogakuin University, Nakanomachi Hachioji, 192-0015, Japan*
[4]*Theoretical Division T-2, Los Alamos National laboratory, Los Alamos, New Mexico 87544, USA*
[5]*Institute of Physics, National Chiao-Tung University, Hsinchu 300, Taiwan*
[6]*Physics Division, National Centre for Theoretical Sciences, Hsinchu 300, Taiwan*
[7]*High Energy Accelerator Research Organization (KEK), Tsukuba 305-0801, Japan*
[8]*Department of Physics, Kyoto University, Kyoto 606-8501, Japan*
[9]*Center for Computational Sciences, University of Tsukuba, Tsukuba, Ibaraki 305-8577, Japan*

(Received 7 March 2009; published 31 August 2009)

We propose a new renormalization scheme of the running coupling constant in general gauge theories using the Wilson loops. The renormalized coupling constant is obtained from the Creutz ratio in lattice simulations and the corresponding perturbative coefficient at the leading order. The latter can be calculated by adopting the zeta-function resummation techniques. We perform a benchmark test of our scheme in quenched QCD with the plaquette gauge action. The running of the coupling constant is determined by applying the step-scaling procedure. Using several methods to improve the statistical accuracy, we show that the running coupling constant can be determined in a wide range of energy scales with a relatively small number of gauge configurations.

DOI: 10.1103/PhysRevD.80.034507 PACS numbers: 11.10.Gh, 11.15.Ha

I. INTRODUCTION

One of the key subjects upon which recent attention has been focused is the flavor dependence of $SU(N)$ Yang-Mills theories. In particular, given a number of flavors N_f, the question is whether the theory has an (approximate) infrared fixed point. This question is triggered by efforts to construct an alternative mechanism of electroweak symmetry breaking, *via* assuming the existence of a new, strongly interacting sector beyond the electroweak scale [1]. The earliest model of this sort, the so-called technicolor [2,3], gives rise to a dynamical electroweak symmetry breaking by introducing a QCD-like sector scaled up to some TeV. While theoretically appealing, the simplest form of the technicolor model and its variants with QCD-like dynamics are ruled out or disfavored by electroweak precision measurements. However, the possibility of such a mechanism with a non-QCD-like theory [4–9] is still open, and may provide observable signatures at the LHC. It is thus an important but challenging task to investigate the low-energy landscape of spontaneously broken, strongly interacting gauge theories [10].

Among the theoretical tools at hand, the numerical approach to lattice gauge theories has made it possible to gain quantitative information about strong dynamics of gauge theories. The current understanding can be summarized as follows. A vectorlike gauge theory, e.g. QCD, is known to exhibit confinement and dynamical chiral symmetry breaking for a small number of massless fermions, N_f, in the fundamental representation of the gauge group. When N_f is just below the value N_f^{af} at which the asymptotic freedom sets in, the theory is conformal (unbroken chiral symmetry, no confinement) in the infrared. Such a theory is believed to remain conformal down to some critical value N_f^c, where the coupling becomes strong enough and the transition to the confined chirally broken phase occurs. The range $N_f^c \leq N_f \leq N_f^{af}$ is called the *conformal window.*

It is thus essential to investigate strongly interacting gauge theories in a wide range of parameters, such as the number of colors, the number of flavors, and the fermion representations [11]. Several modern lattice studies in this research direction have recently been performed [12–24]. In particular, the authors of Refs. [13,23] performed the calculation of the running coupling constant using the Schrödinger functional scheme, and found evidence for an infrared fixed point in $SU(3)$ gauge theory with $N_f = 12$. However, it is important to study the running coupling constant in different renormalization schemes in order to conclude that the fixed point is not an artifact due to a particular renormalization prescription but a physical one. For this purpose, we propose a new renormalization

*erek.bilgici@uni-graz.at
†flachi@yukawa.kyoto-u.ac.jp
‡itou@yukawa.kyoto-u.ac.jp
§kurachi@lanl.gov
‖dlin@mail.nctu.edu.tw
¶hideo.matsufuru@kek.jp
**ohki@yukawa.kyoto-u.ac.jp
††onogi@yukawa.kyoto-u.ac.jp
‡‡yamazaki@ccs.tsukuba.ac.jp

scheme which uses the Wilson loops (WL) as a key ingredient. Such a scheme is applicable to general gauge theories as long as the Wilson loops can be defined, and provides an efficient computational method for lattice gauge theories. Specifically, a renormalized amplitude is defined as the ratio among the Wilson loops, namely, the Creutz ratio, and its perturbative counterpart. The former can be evaluated nonperturbatively by the Monte Carlo simulation, while the latter calculated analytically once the underlying theory is specified. By properly defining the nonperturbatively renormalized coupling constant, its scale dependence is extracted using the step-scaling procedure, i.e., from the volume dependence of the coupling [25].

Applying our scheme will provide not only an independent check on the extent of the conformal window, but also several computational advantages. The Creutz ratio can be obtained without $O(a)$ discretization errors, provided these errors are absent in the lattice action. This means our scheme is in principle free from any $O(a)$ systematic effect. Furthermore, this scheme only involves simple gluonic observables, therefore does not introduce any particular kinematical setup which can deteriorate the discretization error or break chiral symmetry. Therefore it can be applied to simulations with dynamical fermions of any type, without restrictions on N_f. For these features, this scheme may be an attractive alternative to the Schrödinger functional scheme or the twisted Polyakov loop scheme [26–28].

Before performing calculations for the gauge theories with dynamical fermions, as a benchmark test, we apply this new scheme to the computation of the running coupling constant in quenched lattice QCD. The numerical calculation is performed using the plaquette gauge action with periodic boundary conditions. These boundary conditions are chosen for simplicity. Nevertheless, it results in effects of degenerate vacua known as the ''toron'' [29]. Our scheme can, however, be applied in principle to any choice of boundary conditions, such as twisted boundary conditions, which ensure no unwanted zero-mode contributions by inducing nontrivial background configurations. Adopting several methods to improve statistical accuracy, we can determine the running of the coupling constant in a wide range of energy scales with a relatively small number of gauge configurations.

Another essential ingredient of our scheme is the perturbative calculation of the renormalization constant. This is performed analytically using zeta-function resummation techniques, which prove to be quite convenient. First of all, zeta-function techniques offer a natural method to study the analyticity (and regularity) properties of the perturbative counterpart of the Creutz ratio. In addition, some algebraic rearrangements of zeta functions, originally due to Chowla and Selberg [30], allow us to recast the expressions in terms of analytic functions accompanied by some exponentially converging series, whose evaluation is almost trivial and requires little computer power. The zeta-function methods we apply can be easily extended to any boundary conditions and to the case of the Polyakov lines [31].

This paper is organized as follows. In the next section we give the definition of the new scheme. The perturbative calculation is illustrated in Sec. III. Section IV is devoted to the details of our numerical simulations, after a brief introduction to the step-scaling procedure. Section V contains a discussion on the numerical results and a comparison with other results in the literature. Finally, Sec. VI summarizes our conclusions. The paper contains two appendices where technical details and simulation parameters are reported. Preliminary results of this work have been presented in Ref. [32].

II. WILSON-LOOP SCHEME

In this section, we define a new renormalization scheme, the ''*Wilson-loop scheme*.'' Let us consider an amplitude $\mathcal{A}$ whose tree-level approximation is

$$\mathcal{A}^{\text{tree}} = k g_0^2, \tag{2.1}$$

where g_0 is the bare coupling constant, and k is a coefficient of proportionality that does not depend on g_0 and can be explicitly calculated for a given underlying theory. With a nonperturbatively calculated amplitude $\mathcal{A}^{\text{NP}}$ at the scale μ, the renormalization constant $Z(\mu) \equiv \mathcal{A}^{\text{NP}}(\mu)/\mathcal{A}^{\text{tree}}$ relates the renormalized coupling constant, $g(\mu)$, to the bare one, leading to the relation

$$g^2(\mu) = \frac{\mathcal{A}^{\text{NP}}(\mu)}{k}. \tag{2.2}$$

Although in particle physics an S-matrix element, i.e. a scattering amplitude, is usually adopted as $\mathcal{A}$, to define $g(\mu)$ one can equivalently use any physical quantity that can be perturbatively expanded and is proportional to g_0^2 at the tree level.

We define the Wilson-loop scheme by taking the ''amplitude'' to be

$$\mathcal{A}_W(R; L_0; g_0) \equiv -R^2 \frac{\partial^2}{\partial R \partial T} \times \ln\langle W(R, T; L_0, T_0)\rangle|_{T=R; T_0=L_0}, \tag{2.3}$$

where $W(R, T; L_0, T_0)$ is the Wilson loop with the temporal and spatial sizes T and R, on a lattice of the physical size $L_0^3 \times T_0$. In this work, we take T_0 to be the same as L_0, and drop it in the argument of the Wilson loop. The scale L_0 will be identified as the renormalization scale later. On a finite lattice, W, and thus $\mathcal{A}_W$, also depend on the lattice spacing a which is determined by the bare coupling g_0. The dependence of $\mathcal{A}_W$ on a is removed by taking the con-

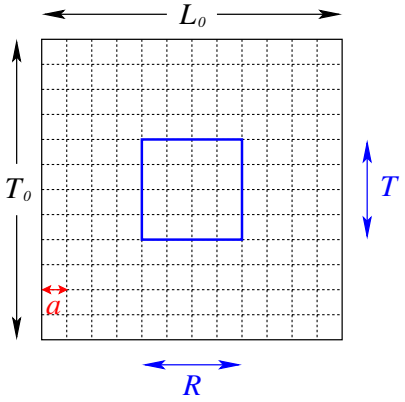

FIG. 1 (color online). Wilson loop defined on the latticized space-time box. T_0, L_0 and T, R represent the size of the box and the Wilson loop in the temporal and spatial directions, respectively; a is the lattice spacing.

tinuum limit, $a \to 0$. A pictorial definition of the Wilson loop is shown in Fig. 1.

Using lattice perturbation theory (see Fig. 2), $\mathcal{A}_W$ can be shown to be proportional to g_0^2 at the lowest order. Thus, once the value of k is calculated, relation (2.2) leads to, after taking the continuum limit, a prescription to obtain the renormalized coupling:

$$g^2\left(L_0, \frac{R}{L_0}\right) = -\frac{R^2}{k(R/L_0)} \frac{\partial^2}{\partial R \partial T} \ln\langle W(R, T; L_0)\rangle^{\mathrm{NP}}|_{T=R}. \tag{2.4}$$

In the above expression we have made explicit that in the continuum limit k is a *regular* function of R/L_0 only. This will be proved in the next section. The remaining factor on the right hand side of Eq. (2.4) can be evaluated on the lattice as the Creutz ratio

$$\chi(\hat{R} + 1/2; L_0/a) = -\ln\left(\frac{W(\hat{R}+1, \hat{T}+1; L_0/a) W(\hat{R}, \hat{T}; L_0/a)}{W(\hat{R}+1, \hat{T}; L_0/a) W(\hat{R}, \hat{T}+1; L_0/a)}\right)\Bigg|_{\hat{T}=\hat{R}}, \tag{2.5}$$

where $\hat{T} \equiv T/a$ and $\hat{R} \equiv R/a$. The value of χ is evaluated by a Monte Carlo simulation.

The renormalized coupling constant in the Wilson-loop scheme can be written as

$$g_w^2\left(L_0, \frac{R + a/2}{L_0}, \frac{a}{L_0}\right) = (\hat{R} + 1/2)^2 \cdot \chi(\hat{R} + 1/2; L_0/a)/k. \tag{2.6}$$

The quantity g_w^2 depends on three different scales, L_0, R, and a; by taking the ratio to L_0, we use $r \equiv (R + a/2)/L_0$, a/L_0, and L_0 as the independent parameters. Fixing r to a specific value means fixing the renormalization scheme. The ratio a/L_0 specifies the discretization of the box, and can be removed by taking the continuum limit, $a/L_0 \to 0$. After fixing the two dimensionless parameters r and a/L_0, g_w^2 becomes a function of a single scale, L_0. In our scheme, following the step-scaling procedure, L_0 is identified as the scale at which the renormalized coupling is defined.

There are several advantages in using the Wilson-loop scheme. An evident one is that our scheme does not contain $O(a)$ systematic effects as long as they are absent in the lattice action. This is because the Creutz ratio is free from $O(a)$ discretization errors, due to the automatic $O(a)$ improvements of the heavy quark propagator after the redefinition of the mass and the wave function [33]. This is in contrast to the case of the Schrödinger functional scheme, in which the boundary counter terms give rise to additional $O(a)$ systematic errors. Such a particular kinematical setup also breaks chiral symmetry. Furthermore, this scheme only involves simple gluonic observables and can be easily applied to the case with any type of dynamical fermions without restriction to the number of flavors.

III. COMPUTATION OF k

One of the indispensable ingredients of the scheme presented in the previous section is the calculation of the coefficient k in Eq. (2.1). It can be generically split into two terms:

$$k = k_0 + k_1, \tag{3.1}$$

where k_0 represents the zero-mode contribution, while k_1 can be expressed as

$$k_1 = -2R^2 C_F \frac{\partial^2}{\partial R \partial T}\left[\frac{4}{(2\pi)^4} \sum_n{}' \left(\frac{\sin\frac{\pi n_0 T}{L_0}}{n_0}\right)^2 \frac{e^{i(2\pi n_3 R/L_0)}}{n^2}\right]_{T=R}, \tag{3.2}$$

where the summation is taken over integer values of n_i ($i = 0, \ldots, 3$) except for the case $n_0 = n_1 = n_2 = n_3 = 0$ (indicated by the prime in the sum), and $n^2 \equiv n_0^2 + n_1^2 + n_2^2 + n_3^2$. The zero-mode contribution depends on the

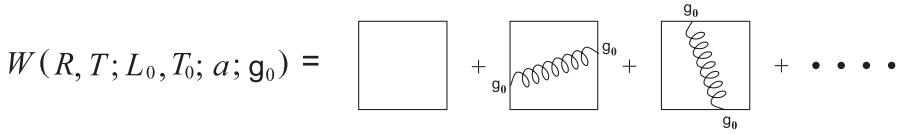

FIG. 2. Schematic illustration of the perturbative expansion of the Wilson loop.

boundary conditions. In the following, we will concentrate on the case of periodic boundary conditions. In this case, k_0 was initially calculated in Ref. [29]. For $SU(3)$ gauge group, k_0 is given by

$$k_0 = \frac{2}{3} C_F \left(\frac{R}{L_0}\right)^4. \tag{3.3}$$

The scope of this section is to present a method to compute the quantity k. The method we develop will be illustrated for the case of periodic boundary conditions, but it can be applied, with minor changes, to the case of twisted or mixed boundary conditions. As we have seen, the contribution from the zero mode, k_0, can be separated from the rest and is obviously regular. Thus to compute (and to prove the regularity of) k, we only need to consider k_1. Our starting point is the quantity:

$$S(T/L_0, R/L_0) \equiv \sum_{n_0=-\infty}^{\infty} \frac{\sin\frac{2\pi T}{L_0} n_0}{n_0} \times \left[2 \sum_{n_1,n_2} \sum_{n_3=1}^{\infty} \frac{\cos\frac{2\pi R}{L_0} n_3}{n_0^2 + n_1^2 + n_2^2 + n_3^2} + \sum_{n_1,n_2}{}' \frac{1}{n_0^2 + n_1^2 + n_2^2} \right]. \tag{3.4}$$

k_1 can be obtained from $S(T/L_0, R/L_0)$ *via*

$$k_1 = -\frac{R^2 C_F}{2\pi^3 L_0} \frac{\partial S}{\partial R}(T/L_0, R/L_0).$$

Although it is not possible to find a closed form for $S(T/L_0, R/L_0)$ in terms of elementary functions, the use of zeta-function resummation techniques and basic analytic continuation allows us to recast $S(T/L_0, R/L_0)$ into the form of a practically computable quantity, and to prove the regularity of k through an explicit calculation. The computation is carried out in a few steps. The first is the evaluation of the sum over n_3 by using the Poisson summation formula. Then, the summation over n_1 and n_2, is written in terms of the Epstein zeta functions. After these steps, the expression of $S(T/L_0, R/L_0)$ becomes compact. However, without further rearrangements, it is of little practical use. To this aim, it is convenient to rewrite the Epstein zeta functions using the Chowla-Selberg formula that renders the zeta functions into the form of elementary analytic functions plus some rapidly converging series. The subsequent step is to analytically perform the integrals introduced when using the Poisson summation formula, and finally perform the remaining summations numerically. Although the above procedure may seem involved, the actual implementation is rather simple. The method has also the bonus of providing a proof of the regularity of the Creutz ratio, as we will explicitly show in the following.

The first step of our procedure is to employ the Poisson summation formula:

$$\sum_{n_3=1}^{\infty} f(n_3) = -\frac{1}{2} f(0) + \int_0^{\infty} dt f(t) + 2 \sum_{n=1}^{\infty} \int_0^{\infty} f(t) \cos(2\pi n t) dt. \tag{3.5}$$

A straightforward application of the above relation to the function $S(T/L_0, R/L_0)$ gives:

$$S(T/L_0, R/L_0) = 2 \sum_{n_0=-\infty}^{\infty} \frac{\sin\frac{2\pi T}{L_0} n_0}{n_0} \sum_{m=-\infty}^{\infty} \int_0^{\infty} \cos(2\pi(m + R/L_0)t) \zeta_t(s; n_0) dt, \tag{3.6}$$

where we have used the standard definition of the generalized Epstein zeta function:

$$\zeta_t(s; n_0) \equiv \sum_{n_1=-\infty}^{\infty} \sum_{n_2=-\infty}^{\infty} (n_0^2 + n_1^2 + n_2^2 + t^2)^{-s}. \tag{3.7}$$

The parameter s is a regulator, introduced to perform the necessary analytical continuations. The limit $s \to 1$ will be taken at the end of the calculation. It is interesting that the function $S(T/L_0, R/L_0)$ can be entirely written in terms of the integral function

$$\mathcal{Z}(\Omega) = \int_0^{\infty} \cos(2\pi\Omega t) \zeta_t(s; n_0) dt. \tag{3.8}$$

Although compact, the result Eq. (3.6) requires further manipulation. A useful way to handle these functions is to make use of the Chowla-Selberg formula. Refs. [34,35] develop the appropriate formalism that allows us to express $\zeta_t(s; n_0)$ as the sum of analytic functions plus a rapidly converging series:

$$\zeta_t(s; n_0) = \pi \frac{\Gamma(s-1)}{\Gamma(s)} |n_0^2 + t^2|^{(1-s)} + \frac{2\pi}{\Gamma(s)} \sum_{p,q=-\infty}^{\infty\prime} [\pi^2(p^2 + q^2)]^{-(1-s)/2} \times (n_0^2 + t^2)^{(1-s)/2} K_{1-s}(2\pi\sqrt{n_0^2 + t^2}\sqrt{p^2 + q^2}). \tag{3.9}$$

The other tool is the following integral formula (see Ref. [36]):

$$\int_0^\infty \cos(2\pi\Omega t)(t^2+n_0^2)^{(1-s)/2}K_{1-s}(2\pi(p^2+q^2)^{1/2}(t^2+n_0^2)^{1/2})dt$$
$$=\sqrt{\frac{\pi}{2}}(2\pi\sqrt{p^2+q^2})^{1-s}n_0^{1/2+(1-s)}(4\pi^2(\Omega^2+p^2+q^2))^{((s-1)/2)-(1/4)}K_{(s-1)-1/2}(2\pi n_0\sqrt{(p^2+q^2)+\Omega^2}). \quad (3.10)$$

The procedure is now straightforward and consists in using the relations (3.9) and (3.10) in Eq. (3.6). Some computations lead to

$$Z(\Omega)=\frac{\sqrt{\pi}\Gamma(2-s)}{\Gamma(s)}2\Gamma(s-1)\cos(\pi((1-s)+1/2))\left(\frac{n_0}{\pi\Omega}\right)^{(1-s)+1/2}K_{(s-1)-1/2}(2\pi\Omega n_0)+(2\pi)^{3/2}\frac{2^{-s}}{\Gamma(s)}$$
$$\times\sum_{p,q=-\infty}^{\infty\prime} n_0^{1/2+(1-s)}[4\pi^2(p^2+q^2+\Omega^2)]^{(s-1)/2-1/4}K_{(s-1)-1/2}[2\pi n_0(p^2+q^2+\Omega^2)]^{1/2}. \quad (3.11)$$

It can be easily checked that, in the above expression, the limit $s\to 1$ can be taken safely giving

$$\mathcal{Z}(\Omega)=\frac{\pi}{2|\Omega|}e^{-2\pi|\Omega|n_0}+\frac{\pi}{2}\sum_{p,q=-\infty}^{\infty\prime}(p^2+q^2+\Omega^2)^{-1/2}e^{-2\pi n_0\sqrt{p^2+q^2+\Omega^2}}. \quad (3.12)$$

It is evident that the quantity $\mathcal{Z}(\Omega)$ is regular. We can now substitute Eq. (3.12) into Eq. (3.4), and rearrange it as

$$S(T/L_0,R/L_0)=\frac{4\pi^2T}{L_0}[S_0(R/L_0)+S_1(T/L_0,R/L_0)], \quad (3.13)$$

where we have separated the $n_0=0$ contribution from the remaining part which is exponentially suppressed. This separation leads to the definition

$$S_0(R/L_0)=A_1(R/L_0)+A_2(R/L_0)+A_3(R/L_0), \quad (3.14)$$

$$S_1(T/L_0,R/L_0)=B_1(T/L_0,R/L_0)+B_2(T/L_0,R/L_0)+B_3(T/L_0,R/L_0), \quad (3.15)$$

where

$$A_1(R/L_0)\equiv\sum_{m=-\infty}^{+\infty}\frac{1}{2|m+(R/L_0)|}, \quad (3.16)$$

$$A_2(R/L_0)\equiv 2\sum_{m=-\infty}^{+\infty}\sum_{p,q=1}^{\infty}\frac{1}{(p^2+q^2+|m+(R/L_0)|^2)^{1/2}}, \quad (3.17)$$

$$A_3(R/L_0)\equiv 2\sum_{m=-\infty}^{+\infty}\sum_{p=1}^{\infty}\frac{1}{(p^2+|m+(R/L_0)|^2)^{1/2}}, \quad (3.18)$$

$$B_1(T/L_0,R/L_0)\equiv\sum_{n_0=1}^{\infty}\frac{\sin\frac{2\pi T}{L_0}n_0}{\pi n_0T/L_0}\sum_{m=-\infty}^{+\infty}\frac{e^{-2\pi|m+(R/L_0)|n_0}}{2|m+(R/L_0)|}, \quad (3.19)$$

$$B_2(T/L_0,R/L_0)\equiv 2\sum_{n_0=1}^{\infty}\frac{\sin\frac{2\pi T}{L_0}n_0}{\pi n_0T/L_0}\sum_{m=-\infty}^{+\infty}\sum_{p,q=1}^{\infty}\times\frac{e^{-2\pi n_0\sqrt{p^2+q^2+|m+(R/L_0)|^2}}}{(p^2+q^2+|m+(R/L_0)|^2)^{1/2}}, \quad (3.20)$$

$$B_3(T/L_0,R/L_0)\equiv 2\sum_{n_0=1}^{\infty}\frac{\sin\frac{2\pi T}{L_0}n_0}{\pi n_0T/L_0}\sum_{m=-\infty}^{+\infty}\sum_{p=1}^{\infty}\times\frac{e^{-2\pi n_0\sqrt{p^2+|m+(R/L_0)|^2}}}{(p^2+|m+(R/L_0)|^2)^{1/2}}. \quad (3.21)$$

Because of the exponential suppression, the terms B_1, B_2, and B_3, and thus $S_1(T/L_0,R/L_0)$, are clearly regular. Therefore, to prove the regularity of k, we only have to show that $S_0(R/L_0)$ is also regular. To show that the terms (3.16), (3.17), and (3.18) also lead to a regular expression for $S_0(R/L_0)$ (and to compute them), it requires further manipulations.

The first term, (3.16), can be computed analytically:

$$A_1(R/L_0)=\frac{1}{2}\left[-\frac{L_0}{R}-\psi(R/L_0)+\psi(-R/L_0)\right], \quad (3.22)$$

where $\psi(x)$ is the Euler psi function [36]. The remaining two terms, A_2 and A_3, can be rearranged by performing first the summation over m, and then by using the Chowla-Selberg formula. We leave the details in Appendix A, and present the results here:

$$A_2(R/L_0)=8\sum_{j=1}^{\infty}\cos(2j\pi R/L_0)K_0(2j\pi\sqrt{p^2+q^2})+(R\text{-independent terms}), \quad (3.23)$$

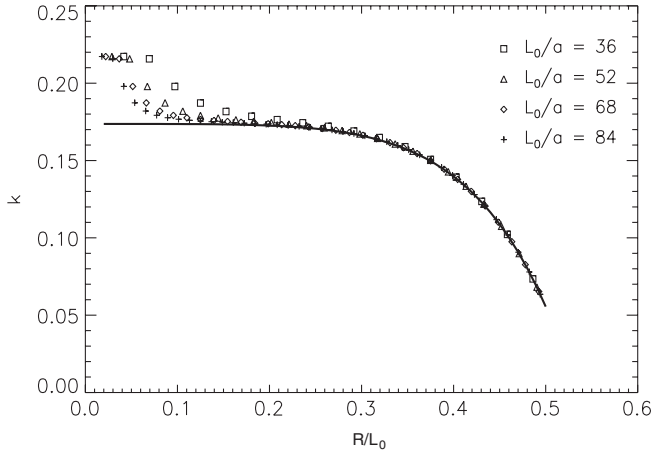

FIG. 3. The figure shows the dependence of k on R/L_0. The solid line represents k, in the continuum limit, according to the analytical expressions given in the text. The squares are results obtained using numerical lattice calculation for the sum in Eq. (3.2). As can be seen from the figure, the (continuum) limit of k for $L_0/a \to \infty$ exists and is finite. Also, the convergence of the lattice computation to the continuum value is faster for larger values of R/L_0.

$$A_3(R/L_0) = 8 \sum_{q,j=1}^{\infty} \cos(2j\pi R/L_0) K_0(2j\pi q) + (R\text{-independent terms}). \tag{3.24}$$

Written as above, it is a trivial matter to see that, after taking the derivative of A_1, A_2, and A_3 with respect to R, $S_0(R/L_0)$, and thus k, is nicely behaved due to the exponential falloff of the Kelvin functions $K_\nu(z)$.

The last step of our procedure consists in evaluating the above expressions. The numerical computation of the sums in Eqs. (3.19), (3.20), (3.21), (3.22), and (3.24), does not present any problem due to the exponential suppression. Differentiating with respect to R, substituting $T/L_0 = R/L_0$, and combining the results according to Eqs. (3.2), (3.3), and (3.4) lead to the result for k. Figure 3 shows the dependence of the function k with respect to R/L_0. Table I provides some indicative values for k.

IV. NUMERICAL SIMULATION

In this section, we will describe the details of our numerical simulations. For later use, we define the coupling-squared, $\tilde{g}_w^2$,

$$\tilde{g}_w^2\left(\beta, r, \frac{L_0}{a}\right) \equiv k g_w^2, \tag{4.1}$$

where $r \equiv (R + a/2)/L_0$. Note that we express $\tilde{g}_w^2$ as a function of β, r, and a/L_0 instead of L_0, r, and L_0/a. The above redefinition is chosen for convenience, since β, r, and a/L_0 are the actual input parameters for the simulations.

TABLE I. Values for k from the continuum calculation.

R/L_0	k	R/L_0	k
0.02	0.173 65	0.30	0.166 08
0.10	0.173 60	0.35	0.156 94
0.15	0.173 36	0.40	0.139 70
0.20	0.172 59	0.45	0.108 85
0.25	0.170 58	0.50	0.055 56

A. Step scaling

We begin by briefly reviewing the step-scaling procedure (see Refs. [25,37,38] for details), that we use to evaluate the evolution of the running coupling in a wide range of the energy scale on the lattice.

The first step is to fix a value for r, and find a set of parameters, $(\beta, L_0/a)$, which produce the same value of $\tilde{g}_w^2$ for several different choices of L_0/a:

$$\{(\beta_1^{(1)}, (L_0/a)_1^{(1)}), (\beta_2^{(1)}, (L_0/a)_2^{(1)}), \ldots\}. \tag{4.2}$$

We achieve this by tuning the value of β in such a way that the physical volume L_0 is fixed for different values of L_0/a. We denote this fixed physical volume for the starting point of the step-scaling procedure by $\tilde{L}_0$.

The next step is to vary the physical volume from $\tilde{L}_0$ to $s\tilde{L}_0$, which gives the evolution of the running coupling from the energy scale $\tilde{L}_0^{-1}$ to $(s\tilde{L}_0)^{-1}$, where s is the scaling factor. This step can be performed by changing the lattice size from $(L_0/a)^{(1)}$ to $s(L_0/a)^{(1)}$, leaving each value of $\beta^{(1)}$ unchanged. Values of g_w^2 calculated with these new parameter sets should be considered as the coupling at the energy scale $(s\tilde{L}_0)^{-1}$ up to discretization errors, and the extrapolation to the continuum limit can be taken

$$g_R^2\left(\frac{1}{s\tilde{L}_0}\right) \equiv \lim_{a\to 0}\left[Z\left(\frac{1}{s\tilde{L}_0}, \frac{a}{s\tilde{L}_0}\right) g_0^2(a)\right], \tag{4.3}$$

where Z is the renormalization factor as defined below Eq. (2.1). The resultant value of the coupling, g_R^2, should be considered as the renormalized coupling at the energy scale $(s\tilde{L}_0)^{-1}$. This is the way to obtain a single discrete step of evolution of the running coupling with scaling factor s.

Next, we find a new parameter set for $(\beta^{(2)}, (L_0/a)^{(2)})$, which reproduces the value of $g_w^2(1/s\tilde{L}_0)$ obtained in the previous step. Here, we chose the parameter set in such a way that the new lattice size $(L_0/a)^{(2)}$ is equal to the original one, $(L_0/a)^{(1)}$. From here, we can repeat exactly the same procedure described so far: we calculate g_w^2 with the parameter set $(\beta^{(2)}, s(L_0/a)^{(1)})$. By iterating this procedure n times, we obtain the evolution of the running coupling from the energy scale $1/\tilde{L}_0$ to $(s^n\tilde{L}_0)^{-1}$.

B. Simulation parameters

We use the standard Wilson plaquette gauge action defined on a four-dimensional Euclidean lattice with finite volume L_0^4. In this work, we adopt untwisted periodic boundary conditions. However, it is straightforward to use other boundary conditions (e.g., twisted boundary conditions) when necessary. Gauge configurations are generated by using the pseudoheatbath algorithm with over-relaxation, mixed in the ratio of 1:5. In the remainder of this paper, we use the word "a sweep" to refer to the combination of one pseudoheatbath update sweep followed by five over-relaxation sweeps. In order to eliminate the influence of autocorrelation, we either take large enough number of sweeps between measurements, or adopt the method of binning with a large enough size of bin to estimate the statistical error reliably. We perform the numerical simulations based on the step-scaling procedure explained in the previous section for a fixed value $r = 0.3$. (The reason for this choice will be given in the next subsection.) We set the scaling parameter $s = 1.5$ with five different starting lattice sizes being $\frac{L_0}{a} = 10$, 12, 14, 16, and 18, which means lattice sizes after the scaling at each step are $\frac{L_0}{a} = 15$, 18, 21, 24, and 27, respectively. We take $\tilde{g}_w^2 = 0.2871$ (which corresponds to $g_w^2 = \frac{\tilde{g}_w^2}{k(r=0.3)} \simeq 1.728$) as the starting value of the first step of the step-scaling procedure. Tunings of the values of β (namely, finding values of β which satisfy $\tilde{g}_w^2(\beta, r = 0.3, \frac{L_0}{a}) = 0.2871$ for each $\frac{L_0}{a} = 10$, 12, 14, 16, and 18 in the first step) are carried out by interpolating the data obtained from simulations for different values of L_0/a and β shown in Fig. 4. Each data point in the figure is calculated from 200 gauge configurations with a 1000-sweep separation between configurations. Once we obtain values of β which reproduce $\tilde{g}_w^2(\beta, r = 0.3, \frac{L_0}{a}) = 0.2871$ for $\frac{L_0}{a} = 10$, 12, 14, 16, and 18, we carry out simulation for $s = 1.5$ step scaling, namely, simulations for $\frac{L_0}{a} = 15$, 18, 21, 24, and 27

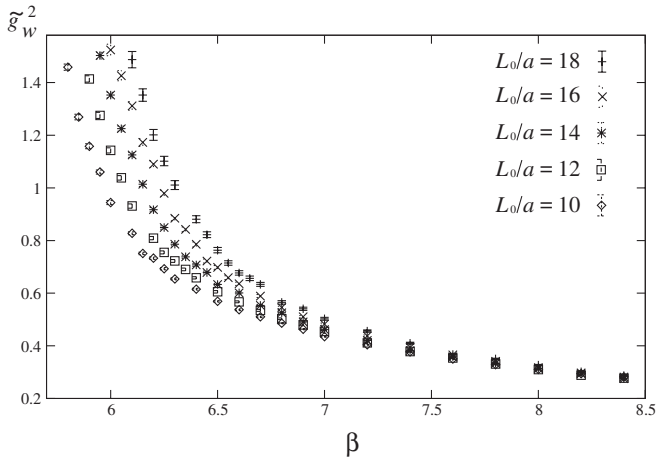

FIG. 4. $\tilde{g}_w^2$ obtained from simulations for different values of L_0/a and β.

with the values of β we tuned. These results are used to take the continuum limit, then the resultant value of $\tilde{g}_w^2$ becomes a starting value for the next step. We iterate this procedure 7 times. The combination of L_0/a and β used for the simulations are shown in Table II.[1]

C. Simulation details

There are several practical steps to calculate the quantity $\tilde{g}_w^2(\beta, r, L_0/a)$ from numerical simulations. Here we explain various technical details of our computations.

We use the APE smearing [39] of link variables defined by the following equation:

$$U_{x,\mu}^{(n+1)} = \mathrm{Proj}_{SU(3)}\left[U_{x,\mu}^{(n)} + \frac{1}{c}\Sigma_{\mu\neq\nu}^{4} U_{x,\nu}^{(n)} U_{x+\nu,\mu}^{(n)} U_{x+\mu,\nu}^{(n)\dagger} \right], \tag{4.4}$$

where n and c denote the smearing level and the smearing parameter, respectively. The smearing is done for links in all four directions. The result does not depend on the value of c significantly, and we take $c = 2.3$ in the present study. Here, we need to find the optimal values of $r \equiv \frac{R+a/2}{L_0}$ and the smearing level n, by considering the following requirements. For better control of discretization error, it is preferable to choose a larger value of r. Meanwhile, for the purpose of reducing the statistical error, it is better to take a smaller value of r and higher number of n. Figure 5 shows the smearing-level dependence of $\tilde{g}_w^2$ in the case of $\beta = 8.25$ and $L_0/a = 18$ as an example. From this figure, we find the statistical error is notably reduced even at the smearing-level one. In order to avoid over smearing, n should be smaller than $\hat{R}/2$. This condition leads to the lower bound, $L_0/a > (4n + 1)/(2r)$. We summarize the bound from this requirement in Table III. We observe (see Fig. 5 for the example of the case $L_0/a = 18$ at $\beta = 8.25$) that the data of $(\hat{R} + 1/2) = 1.5$ and 2.5 in a higher smearing level are not reliable because of over smearing. By considering all the above requirements, we find that $(r, n) = (0.3, 1)$ is the optimal choice.

Once we fix the value of r ($r = 0.3$ in our current study), we need to estimate the value of $\tilde{g}_w^2$ for noninteger $\hat{R}$. We interpolate the value of $\tilde{g}_w^2$ using a quadratic function:

$$f(\hat{R} + 1/2) = c_0 + c_1(\hat{R} + 1/2) + c_2(\hat{R} + 1/2)^2, \tag{4.5}$$

with interpolation ranges for each lattice size listed in

[1]The values of β in Table II have numerical ambiguities coming from the statistical errors of the data used for the interpolation. These ambiguities propagate to the error of the physical scale at each step which we are trying to fix. However, it turned out that the effect of that fluctuation to the result of simulation for $s = 1.5$ at each lattice size was negligibly small compared to the statistical error of the simulation itself. Thus, we ignore those errors and resultant fluctuation of the physical scale in the rest of our analysis.

TABLE II. Parameter sets, L_0/a and β, used for the simulation.

Step 1		Step 2		Step 3		Step 4		Step 5		Step 6		Step 7	
L_0/a	β	L_0/a	β	L_0/a	β	L_0/a	β	L_0/a	β	L_0/a	β	L_0/a	β
15	8.31	15	7.80	15	7.44	15	6.968	15	6.571	15	6.207	15	5.907
18	8.25	18	7.83	18	7.45	18	7.040	18	6.656	18	6.303	18	6.000
21	8.27	21	7.86	21	7.49	21	7.076	21	6.734	21	6.377	21	6.087
24	8.32	24	7.91	24	7.55	24	7.156	24	6.797	24	6.463	24	6.170
27	8.40	27	7.97	27	7.61	27	7.243	27	6.871	27	6.546	27	6.229

Table IV. An example is shown in Fig. 5 where $(\hat{R} + 1/2) = 5.4$ corresponds to the interpolation to $r = 0.3$ in the case of $L_0/a = 18$.

The last step of the calculation is to take the continuum limit of $\tilde{g}_w^2$ from data obtained for different combinations of β and L_0/a listed in each column of Table II. We show two example plots in Fig. 6, which are the continuum extrapolations for step 1 and step 7. Since our Wilson-loop scheme does not contain $O(a)$ systematic errors, we extrapolate to the continuum limit using a fit function linear in $(a/L_0)^2$. Four data points ($L_0/a = 27$, 24, 21, and 18) are used for this extrapolation (shown as red solid lines in Fig. 6), and the resultant value is adopted as the central value of $\tilde{g}_w^2$ in the continuum limit. We also take the continuum limit by using a fit function quadratic in $(a/L_0)^2$ with five data points ($L_0/a = 27$, 24, 21, 18, and 15) (indicated by pink dashed curves in Fig. 6), and the difference between the central values of two fits are adopted as the systematic error coming from possible higher order discretization effects. In Fig. 6, we have also plotted extrapolation by a linear function with five points of data for comparison. In this figure, resultant values of the continuum limit obtained from different fit functions are plotted at $(a/L_0)^2 = 0$. (For better visibility, we slightly displaced the data obtained from 5-point quadratic and 5-point linear extrapolations.) All the error bars shown in Fig. 6 are statistical only.

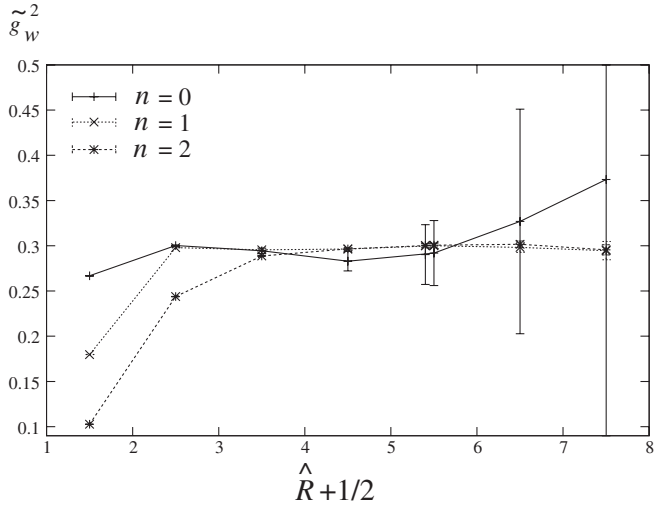

FIG. 5. The values of $\tilde{g}_w^2$ with a statistical error for several values of $(\hat{R} + 1/2)$ in the case of $\beta = 8.25$ and $L_0/a = 18$. Data connected by solid, dotted, and dashed lines denote the data with 0, 1, and 2 smearing levels, respectively.

D. Numerical results

We now show the results of our simulations which were performed using parameters in Table II with procedures explained in the previous section. Details of our parameter choice and numerical results are summarized in Appendix B.

1. Running coupling

In Fig. 7, we plot the resulting values of $\tilde{g}_w^2$ and their statistical errors for $L_0/a = 18$, 21, 24, and 27 for steps 1–7. The continuum limit was taken using a linear function in $(a/L)^2$. In Fig. 7 the values of $\tilde{g}_w^2$ in the continuum-limit are shown with statistical and systematic errors added in quadrature.

The running coupling constant g_w^2 is extracted by dividing $\tilde{g}_w^2$ by $k(r = 0.3) = 0.1661$. The evolution of the running coupling constant is obtained by connecting the resultant values for steps 1–7 by assigning appropriate scales to these steps. We plot the results in Fig. 8. We define the starting energy scale of Step 1 as $1/\tilde{L}_0$, and the evolution of the running coupling constant is plotted as a function of energy in units of $1/\tilde{L}_0$. In this figure, errors are accumulated with the evolution of the running coupling

TABLE III. The lower bound on L_0/a to avoid over smearing.

n	$r = 0.25$	$r = 0.30$	$r = 0.35$
$n = 1$	$L_0/a > 10$	$L_0/a > 8.3$	$L_0/a > 7.1$
$n = 2$	$L_0/a > 18$	$L_0/a > 15$	$L_0/a > 12.8$
$n = 3$	$L_0/a > 26$	$L_0/a > 21.6$	$L_0/a > 18.5$

TABLE IV. Ranges used to interpolate the value of $\tilde{g}_w^2$. The column "$\hat{R} + 1/2$" is the value that corresponds to $r = 0.3$.

L_0/a	$\hat{R} + 1/2$	$\hat{R}_{\min}$	$\hat{R}_{\max}$	L_0/a	$\hat{R} + 1/2$	$\hat{R}_{\min}$	$\hat{R}_{\max}$
10	3.0	2	4	18	5.4	4	6
12	3.6	2	4	21	6.3	5	7
14	4.2	2	5	24	7.2	5	7
16	4.8	3	5	27	8.1	6	8

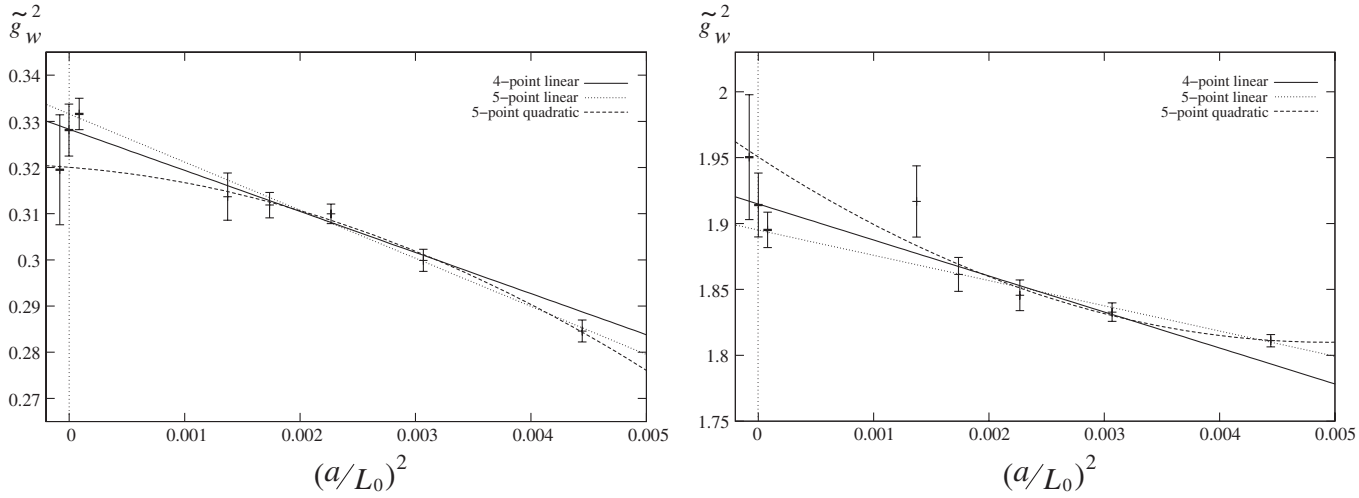

FIG. 6. The continuum limit of $\tilde{g}^2_w$. The left and right panels show Steps 1 and 7, respectively.

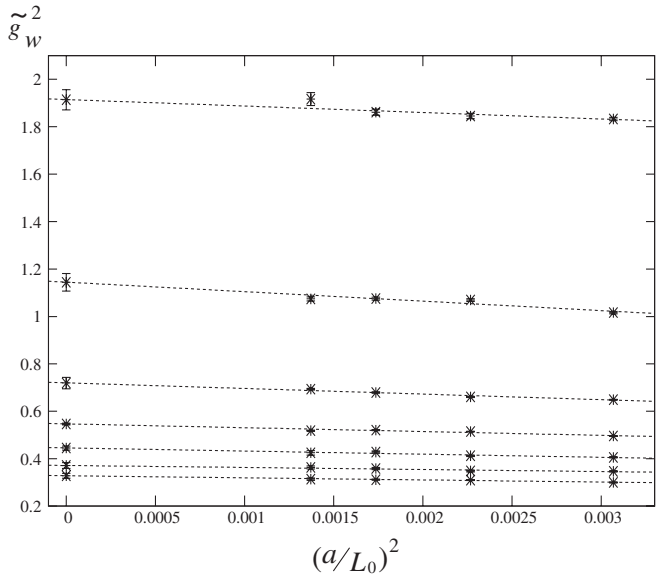

FIG. 7. Results of simulations and the continuum limit of g^2_w in Steps $1 \sim 7$ (from bottom to top).

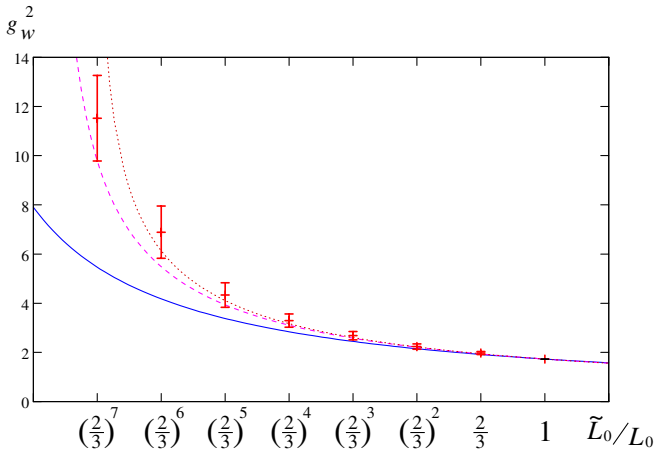

FIG. 8 (color online). Evolution of the running coupling constant in the Wilson-loop scheme, g^2_w, obtained from the step-scaling procedure. The horizontal axis shows the energy scale in units of $1/\tilde{L}_0$. Three curves, from bottom to top, show scheme-independent perturbative running couplings with the one-loop and two-loop approximation, as well as that with the three-loop approximation in the $\overline{\text{MS}}$ scheme.

appropriately[2] in the same way as explained in Ref. [40]. For comparison, we also plot scheme-independent perturbative running couplings with one-loop and two-loop approximation as well as three-loop approximation in the $\overline{\text{MS}}$ scheme (from bottom to top). In the high-energy region, where the perturbative computation is reliable, the Wilson-loop scheme is consistent with the perturbation theory. The figure also shows that our simulation is reaching deep into the low-energy region, in which the perturbative calculation is no longer reliable.

2. Beta function

From the results of the simulation, we can also extract the nonperturbative β function by using the method explained in Ref. [41]. To this end, it is useful to define the step-scaling function in the continuum limit as [40]

$$\sigma(u) = g^2_w(sL), \qquad u \equiv g^2_w(L). \tag{4.6}$$

We list the simulation results for the step-scaling function in Table V. In the week coupling region, $\sigma(u)$ can be perturbatively expanded as [41]

[2]For the appropriate procedure of accumulating error, we need the values of the derivative of the step-scaling function $\sigma(u)$. Here, we used the result of the u^5 polynomial global fitting of $\sigma(u)$ to obtain approximate values of $\sigma'(u)$. See the next subsubsection for details.

TABLE V. Simulation results for the step-scaling function $\sigma(u)$. The values in parentheses represent total errors in units of the last digits.

u	$\sigma(u)$
1.728	1.97(6)
1.97	2.23(7)
2.23	2.68(5)
2.68	3.29(2)
3.29	4.33(14)
4.33	6.89(22)
6.89	11.5(3)

$$\sigma(u) = u + s_0 u^2 + s_1 u^3 + \cdots, \tag{4.7}$$

with the coefficients

$$s_0 = 2b_0 \ln s, \tag{4.8}$$

$$s_1 = (2b_0 \ln s)^2 + 2b_1 \ln s, \tag{4.9}$$

where b_0 and b_1 are the one-loop and the two-loop coefficients of the β function, respectively. In Fig. 9, we plot the data listed in Table V together with the two-loop perturbative curve for $\sigma(u)$ (solid), as well as two curves which are the result of the following two kinds of polynomial fit. For the upper (dashed) curve, we fitted $u + s_0 u^2 + s_1 u^3 + s_2 u^4$ to the data in the range of $u < 5$, and obtained $s_2 = 0.0019(3)$. For the middle (dotted) curve, we fitted $u + s_0 u^2 + s_1 u^3 + s_2 u^4 + s_3 u^5$ to all the data, and obtained $s_2 = 0.0033(6)$ and $s_3 = -0.00048(9)$. As is expected, in the weak coupling region, the data is well explained by the two-loop perturbative result, and polynomial functions fit well to the data also. Meanwhile, the figure clearly shows that neither the two-loop perturbative curve, nor simple polynomial fits can explain the behavior

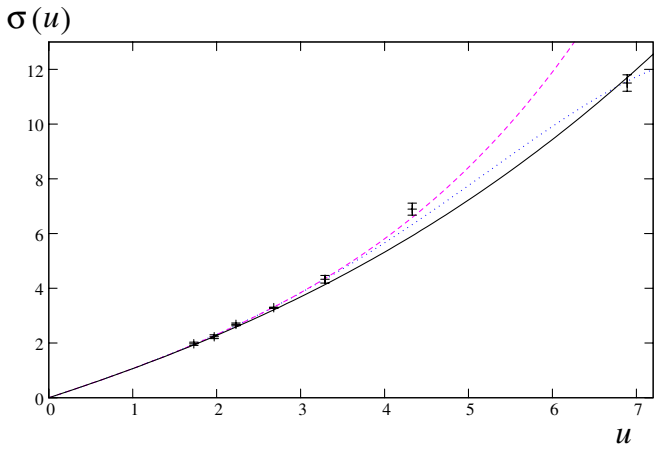

FIG. 9 (color online). Polynomial fit (dashed and dotted curves) of the data for the step-scaling function $\sigma(u)$. The fit ansatz and resultant values of fitting parameters for two curves are explained in the text. The two-loop perturabative curve (solid) is also plotted for comparison.

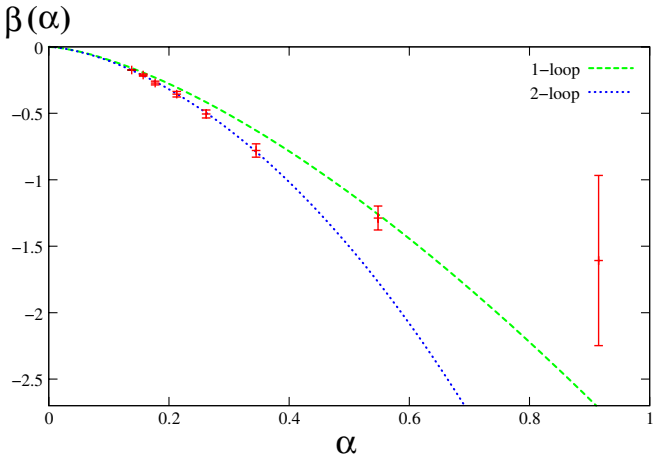

FIG. 10 (color online). Nonperturbative β function in the Wilson-loop scheme. One-loop (green dashed curve) and two-loop (blue dotted curve) perturbative β functions are also plotted for comparison.

of the data in larger values of u. This is nothing but an indication of the emergence of the nonperturbative effect.

The formula to obtain nonperturbative β function from the step-scaling function was given in Ref. [41] as

$$\beta(\sqrt{\sigma(u)}) = \beta(\sqrt{u})\sqrt{\frac{u}{\sigma(u)}}\sigma'(u). \tag{4.10}$$

By applying this formula recursively, we obtained the discrete β function as shown in Fig. 10. Here, while the values of the $\sigma(u)$ are directly given by the results of the simulation,[3] we need to use the result of the fitting to obtain the values of $\sigma'(u)$. To obtain the latter, we adopted the u^5 global fitting explained above. As we noted, it fails to fit to the data in larger values of u, however, as can be seen from the figure, we can expect that it gives *numerically* approximate values. Also, we used the value of the perturbative two-loop approximation for the value of $\beta(u)$ at the smallest u as an initial input value to use Eq. (4.10) recursively. In the figure, we also plotted the one-loop and two-loop perturbative β function for comparison. From this result, we confirmed again that for the smaller coupling region, the data consistently reproduce the perturbative picture, while the nonperturbative effect begins to emerge for larger coupling region.

V. DISCUSSION

We have hitherto concentrated on how the coupling constant runs under the relative change of the scale without referring to its absolute value. The absolute scale can be estimated using the Sommer scale, r_0, defined by

[3]Unlike was done in Ref. [41], we do not have to carry out interpolation in u since we have the data exactly on the value of u that we need.

TABLE VI. The Sommer scale at each β of the Step 7, estimated using Eq. (5.2).

L_0/a	β	r_0/a	$r_0/\tilde{L}_0$
15	5.907	4.543(17)	5.174(19)
18	6.000	5.368(22)	5.096(21)
21	6.087	6.196(27)	5.041(22)
24	6.170	7.040(33)	5.012(23)
27	6.229	7.677(37)	4.858(23)

$$r^2F(r)|_{r=r_0} = 1.65. \tag{5.1}$$

Based on the phenomenological potential models, r_0 corresponds to about 0.5 fm. In this work, however, we use r_0 only to set the reference scale for a comparison with the other scheme. The formula relating β and r_0 is given in Ref. [42],

$$\ln(a/r_0) = -1.6805 - 1.7139(\beta - 6) + 0.8155(\beta - 6)^2 - 0.6667(\beta - 6)^3, \tag{5.2}$$

which is valid in the region $5.7 \leq \beta \leq 6.57$. For our lattices, β values in Step 7 in Table II are in this range. In Table VI, we summarize r_0/a calculated using Eq. (5.2), and the corresponding $r_0/\tilde{L}_0$. In Ref. [42], the values of r_0 in the range $5.7 \leq \beta \leq 6.57$ are determined with errors linearly increasing from 0.3% to 0.6%. These errors are mainly statistical. Since we are only aiming at a rough estimate of the absolute scale in this work, we assign the corresponding size of errors to the results in Table VI. By extrapolation to the continuum limit, we obtain[4]

$$\frac{r_0}{\tilde{L}_0} = 4.75 \pm 0.26. \tag{5.3}$$

Here, the statistical error is negligibly small compared to the systematic error.

We can now estimate the Λ scale in units of r_0. Since it is obvious from Fig. 8 that g_w^2 is well approximated by a two-loop perturbative running coupling at the high-energy region, it is reasonable to estimate the scale Λ by using the value of $g_w^2(1/\tilde{L}_0)$ from the following two-loop relation[5] between $\tilde{L}_0\Lambda$ and $g_w^2(1/\tilde{L}_0)$,

$$\tilde{L}_0\Lambda_{\mathrm{WL}}^{\text{2-loop}} = \mathrm{e}^{-(1/2b_0 g_w^2(1/\tilde{L}_0))}\left(\frac{b_0^2 g_w^2(1/\tilde{L}_0)}{b_0 + b_1 g_w^2(1/\tilde{L}_0)}\right)^{-(b_1/2b_0^2)}, \tag{5.4}$$

where $b_0 = 11/(4\pi)^2$ and $b_1 = 102/(4\pi)^4$ are the one-loop and the two-loop coefficients of the β function of quenched QCD. By substituting the value $g_w^2(1/\tilde{L}_0) = 1.728$, we find

$$\tilde{L}_0\Lambda_{\mathrm{WL}}^{\text{2-loop}} \simeq 0.0399. \tag{5.5}$$

Combining this result with the value of $r_0/\tilde{L}_0$ in Eq. (5.3), we obtain the value of $\Lambda_{\mathrm{WL}}^{\text{2-loop}}$ in units of r_0 as

$$r_0\Lambda_{\mathrm{WL}}^{\text{2-loop}} = 0.190 \pm 0.010. \tag{5.6}$$

We also estimated, in the similar way as above, the value of $r_0\Lambda^{\text{2-loop}}$ in the case of the SF scheme by using the data reported in Ref. [40], and found the following result:

$$r_0\Lambda_{\mathrm{SF}}^{\text{2-loop}} = 0.301 \pm 0.025. \tag{5.7}$$

By fixing r_0 as a reference scale, we obtain the following ratio of $\Lambda_{\mathrm{SF}}^{\text{2-loop}}$ to $\Lambda_{\mathrm{WL}}^{\text{2-loop}}$:

$$\frac{\Lambda_{\mathrm{SF}}^{\text{2-loop}}}{\Lambda_{\mathrm{WL}}^{\text{2-loop}}} = 1.58 \pm 0.16. \tag{5.8}$$

As a consistency check, we have also extracted the ground-state potential from our data at the largest physical volume *via* double exponential fits [43], then used the potential to estimate r_0 and r_c defined as

$$r^2F(r)|_{r=r_c} = 0.65. \tag{5.9}$$

Our results on these quantities are well compatible with those obtained in Ref. [33].

We also estimated the value of $\Lambda_{\mathrm{SF}}^{\text{2-loop}}/\Lambda_{\mathrm{WL}}^{\text{2-loop}}$ without relying on the measurement of any low-energy physical quantity. This can be achieved by comparing results obtained from the same combinations of values of β and L_0/a in the two schemes, with a fixed physical box size L_0 which is much smaller than $1/\Lambda_{\mathrm{QCD}}$. To this purpose, we have carried out simulations using exactly the same values of β and L_0/a as one of the data sets in Ref. [40]. In Table VII, we list the values of the coupling constant in the SF scheme, g_{SF}^2 (which is denoted by $\bar{g}^2$ in Ref. [40]), and results of $\Lambda_{\mathrm{SF}}^{\text{2-loop}}$ estimated from them by using Eq. (5.4). The values of g_w^2 and the corresponding $\Lambda_{\mathrm{WL}}^{\text{2-loop}}$ are also listed in this table.[6] These values result from an interpolation procedure using the data points shown in Fig. 4. The results for $\Lambda_{\mathrm{SF}}^{\text{2-loop}}/\Lambda_{\mathrm{WL}}^{\text{2-loop}}$ at each L_0/a is also listed in the same table. A fit linear in a/L_0 to these results gives the following continuum-limit estimation:

[4]Here we take the continuum limit and estimate the systematic error in the same way as we did in Sec. IV C.

[5]From the difference between two-loop and three-loop β function in the Schrödinger function (SF) scheme, the error in the estimation to Λ due to the higher order effect is about 3%. This is reasonably small compared to other errors in this work.

[6]We notice that the a/L_0 dependence of g_w^2 is rather large partly due to the fact that we used the results of the SF-scheme study as inputs to set the scale for each β. Therefore, the discretization error could be a combination (or the difference) of those from the WL scheme and SF scheme. This error may be dominated by the error from the WL scheme since the effective physical scale is the Wilson-loop size R but not L_0 so that one expects $O((a/R)^2)$ error.

TABLE VII. Values for g^2 and $L_0\Lambda^{2\text{-loop}}$ in the SF and the WL schemes for several sets of L_0/a and β. Results of $g^2_{\rm SF}$ are taken from Ref. [40]. The values in parentheses represent statistical errors in units of the last digits.

L_0/a	β	$g^2_{\rm SF}$	$L_0\Lambda^{2\text{-loop}}_{\rm SF}$	g^2_w	$L_0\Lambda^{2\text{-loop}}_{\rm WL}$	$\Lambda^{2\text{-loop}}_{\rm SF}/\Lambda^{2\text{-loop}}_{\rm WL}$
10	7.8538	1.8776(93)	0.0539(9)	1.9427(68)	0.06043(71)	0.891(18)
12	7.9993	1.8811(38)	0.0542(4)	1.8620(66)	0.05232(65)	1.036(15)
14	8.1380	1.884(11)	0.0545(11)	1.8028(73)	0.04667(68)	1.168(29)
16	8.2500	1.864(10)	0.0525(10)	1.7662(79)	0.04331(72)	1.213(30)

$$\frac{\Lambda^{2\text{-loop}}_{\rm SF}}{\Lambda^{2\text{-loop}}_{\rm WL}} = 1.78 \pm 0.07(\text{stat.}) \pm 0.04(\text{sys.}) \qquad (5.10)$$

Here the systematic error was estimated by the difference between values in the continuum limit with linear and quadratic extrapolations.

A comparison between the results of Eqs. (5.8) and (5.10) shows the ''universality'' of the estimate of $\Lambda^{2\text{-loop}}_{\rm SF}/\Lambda^{2\text{-loop}}_{\rm WL}$, namely, the two different estimates are consistent with each other.[7] From the theoretical point of view, this universality might be a trivial result since quenched QCD has only one scale in the theory. However, from the numerical point of view, it is a rather nontrivial consistency check since one estimation involves the measurement of a low-energy physical quantity while the other is completely from high-energy physics.

We notice that the error of g^2_w is large partly due to the fact that we used the SF as inputs to set the scale for each β. Therefore, the discretization error could be a combination (or the difference) of those from the WL scheme and SF scheme. This error may be dominated by the error from the WL scheme since the effective physical scale is the Wilson-loop size R but not L_0 so that one expects $O((a/R)^2)$ error.

VI. SUMMARY

We proposed a new scheme for the determination of the running coupling on the lattice. Our method is based on the measurement of the finite volume dependence of the Wilson loop. Unlike the SF scheme, our method does not have any $O(a)$ discretization error, therefore the systematic effect arising from the extrapolation to the continuum limit is expected to be quite small. We showed results of numerical study for the quenched QCD as a feasibility test of our scheme. These results confirmed that our method led to the step scaling of the coupling which is consistent with the perturbative running coupling at high energy. We also showed that the coupling calculated by this newly proposed scheme deviates from the two-loop approximation below a certain energy scale. This deviation arises from the effects that are not captured by the two-loop approximation. We have confirmed that our scheme works well for the calculation of the running coupling with a relatively small number of gauge configurations, demonstrating that the statistical error is under control by properly choosing the smearing level and r. We expect that this new method is also applicable to the calculation of the running coupling in other gauge theories, including the $SU(N)$ gauge theory with a large number of dynamical fermions, which will be studied in our future work.

[7]Three-loop perturbative calculation (though quite challenging to carry out it in the WL scheme, while already done in the SF scheme), together with the improvement of systematic and statistical errors, would enable us to perform a even more precise test of this universality by defining the Λ scale with three-loop β function.

ACKNOWLEDGMENTS

We thank Biagio Lucini and Antonio Rago for helpful discussions. We also thank Koichi Yamawaki for organizing a workshop on related topics at Nagoya University, which stimulated our work. This work is supported in part by the Grants-in-Aid of the Ministry of Education (No. 19540286, 19740160, 20039005, 20105002, and 20740133). E. B. is supported by the FWF Doktoratskolleg Hadrons in Vacuum, Nuclei, and Stars (DK W1203-N08). A. F. acknowledges the support of JSPS, Grant No. 19GS0210. M. K. is supported by the Los Alamos National Laboratory under DE-AC52-06NA25396. C.-J. D. L. is supported by the National Science Council of Taiwan *via* Grant No. 96-2112-M-009-020-MY3. During this work, T. Y. has beenthe Yukawa Memorial Foundation. Numerical simulation was carried out on the vector supercomputer NEC SX-8 at YITP, Kyoto University, and SX-8 at RCNP, Osaka University. We are grateful to YITP, Kyoto and NCTS, Hsinchu for their hospitality during the progress of this work.

APPENDIX A: FORMULAS (3.23) AND (3.24)

In the following, we will briefly show how to obtain formulas (3.23) and (3.24). Basically the method we use is a repetition of the generic technique we have adopted in Sec. III: we first perform the sum over m, and then use the Chowla-Selberg formula, which rearranges the expression as a sum of some analytic function plus a series, suppressed by the presence of the Kelvin functions $K_\nu(x)$. For the first term one has:

$$\sum_{m=-\infty}^{+\infty}\sum_{p,q=1}^{\infty}\frac{1}{(p^2+q^2+|m+R/L_0|^2)^s}=\sum_{p,q=1}^{\infty}\Bigg[\frac{\sqrt{\pi}(p^2+q^2)^{(1/2)-s}\Gamma(s-\frac{1}{2})}{\Gamma(s)}+\frac{4\pi^s}{\Gamma(s)}(p^2+q^2)^{(1/4)-(s/2)}\times\sum_{j=1}^{\infty}j^{s-(1/2)}\cos(2j\pi R/L_0)K_{s-(1/2)}(2j\pi\sqrt{p^2+q^2})\Bigg]$$
$$=\sum_{p,q=1}^{\infty}\Bigg[i\frac{\sqrt{\pi}(p^2+q^2)^{(1/2)-s}\Gamma(s-\frac{1}{2})}{\Gamma(s)}+4\sum_{j=1}^{\infty}\cos(2j\pi R/L_0)K_0(2j\pi\sqrt{p^2+q^2})\Bigg]. \tag{A1}$$

In the above formula, the first term disappears upon derivation with respect to R and thus will not contribute to k. The second term is exponentially suppressed due to the presence of $K_0(z)$ and, thus, regular. An analogous procedure applies to $A_3(R/L_0)$:

$$\sum_{m=-\infty}^{+\infty}\sum_{q=1}^{\infty}\frac{1}{(q^2+|m+R/L_0|^2)^s}=\sum_{q=1}^{\infty}\frac{\sqrt{\pi}\Gamma(2s-1)}{\Gamma(\frac{1}{2})}+4\sum_{q,j=1}^{\infty}\cos(2j\pi R/L_0)K_0(2j\pi q). \tag{A2}$$

As before, the first term is independent of R and disappears, when differentiated with respect to R. The second term is exponentially suppressed and regular.

APPENDIX B: SUMMARY OF SIMULATION PARAMETERS AND NUMERICAL RESULTS

Here, we summarize simulation parameters, and numerical results obtained from those simulations. In Tables B.I–B.VII, N_{conf}, N_{sweep}, and $N_{\text{bin size}}$, respectively,

TABLE B.I. Step 1. Continuum limit: $\tilde{g}_w^2 = 0.328 \pm 0.010$.

L_0/a	β	N_{conf}	N_{sweep}	$N_{\text{bin size}}$	$\tilde{g}_w^2$
15	8.31	200	1000	1	0.2846(24)
18	8.25	200	1000	1	0.2999(24)
21	8.27	400	1000	1	0.3100(21)
24	8.32	400	1000	1	0.3119(27)
27	8.40	200	1000	1	0.3137(51)

TABLE B.II. Step 2. Continuum limit: $\tilde{g}_w^2 = 0.371 \pm 0.012$.

L_0/a	β	N_{conf}	N_{sweep}	$N_{\text{bin size}}$	$\tilde{g}_w^2$
15	7.80	200	1000	1	0.3371(26)
18	7.83	200	1000	1	0.3465(29)
21	7.86	200	1000	1	0.3482(36)
24	7.91	200	1000	1	0.3585(48)
27	7.97	200	1000	1	0.3632(66)

TABLE B.III. Step 3. Continuum limit: $\tilde{g}_w^2 = 0.445 \pm 0.009$.

L_0/a	β	N_{conf}	N_{sweep}	$N_{\text{bin size}}$	$\tilde{g}_w^2$
15	7.44	200	1000	1	0.3831(31)
18	7.45	400	1000	1	0.4056(25)
21	7.49	400	1000	1	0.4125(33)
24	7.55	400	1000	1	0.4278(50)
27	7.61	200	1000	1	0.4249(92)

TABLE B.IV. Step 4. Continuum limit: $\tilde{g}_w^2 = 0.547 \pm 0.004$.

L_0/a	β	N_{conf}	N_{sweep}	$N_{\text{bin size}}$	$\tilde{g}_w^2$
15	6.968	10 000	1	100	0.4829(9)
18	7.040	10 000	1	100	0.4959(12)
21	7.076	10 000	1	100	0.5146(15)
24	7.156	10 000	1	100	0.5204(20)
27	7.243	10 000	1	100	0.5181(24)

TABLE B.V. Step 5. Continuum limit: $\tilde{g}_w^2 = 0.719 \pm 0.024$.

L_0/a	β	N_{conf}	N_{sweep}	$N_{\text{bin size}}$	$\tilde{g}_w^2$
15	6.571	10 000	1	100	0.6307(14)
18	6.656	10 000	1	100	0.6489(19)
21	6.734	10 000	1	100	0.6606(27)
24	6.797	10 000	1	100	0.6794(33)
27	6.871	10 000	1	100	0.6931(41)

TABLE B.VI. Step 6. Continuum limit: $\tilde{g}_w^2 = 1.144 \pm 0.037$.

L_0/a	β	N_{conf}	N_{sweep}	$N_{\text{bin size}}$	$\tilde{g}_w^2$
15	6.207	10 000	1	100	0.978(3)
18	6.303	10 000	1	100	1.016(5)
21	6.377	10 000	1	100	1.069(6)
24	6.463	10 000	1	100	1.075(7)
27	6.546	10 000	1	100	1.074(9)

TABLE B.VII. Step 7. Continuum limit: $\tilde{g}_w^2 = 1.914 \pm 0.042$.

L_0/a	β	N_{conf}	N_{sweep}	$N_{\text{bin size}}$	$\tilde{g}_w^2$
15	5.907	10 000	1	100	1.811(5)
18	6.000	10 000	1	100	1.833(7)
21	6.087	10 000	1	100	1.846(12)
24	6.170	10 000	1	100	1.861(13)
27	6.229	10 000	1	100	1.917(27)

represent the number of gauge configurations from which measurement were taken, the number of sweeps between each configurations, and the number of the bin size when we estimate the statistical error. The values in parentheses in the column of $\tilde{g}_w^2$ represent statistical errors in units of the last digits. We also listed the values of $\tilde{g}_w^2$ in the continuum limit with the magnitude of total error at each step.

[1] C. T. Hill and E. H. Simmons, Phys. Rep. **381**, 235 (2003); **390**, 553(E) (2004).
[2] S. Weinberg, Phys. Rev. D **13**, 974 (1976); **19**, 1277 (1979).
[3] L. Susskind, Phys. Rev. D **20**, 2619 (1979).
[4] B. Holdom, Phys. Lett. B **150**, 301 (1985).
[5] K. Yamawaki, M. Bando, and K.-i. Matsumoto, Phys. Rev. Lett. **56**, 1335 (1986).
[6] T. Appelquist, D. Karabali, and L. C. R. Wijewardhana, Phys. Rev. Lett. **57**, 957 (1986); T. Appelquist and L. C. R. Wijewardhana, Phys. Rev. D **35**, 774 (1987); Phys. Rev. D **36**, 568 (1987).
[7] T. Appelquist, J. Terning, and L. C. R. Wijewardhana, Phys. Rev. Lett. **77**, 1214 (1996).
[8] V. Miransky and K. Yamawaki, Phys. Rev. D **55**, 5051 (1997); Phys. Rev. D**56**, 3768(E) (1997); See also V. Miransky and P. Fomin, Sov. J. Part. Nucl. **16**, 203 (1985).
[9] T. Appelquist, A. Ratnaweera, J. Terning, and L. C. R. Wijewardhana, Phys. Rev. D **58**, 105017 (1998).
[10] An early paper on the phase structure of vectorial gauge theories is T. Banks and A. Zaks, Nucl. Phys. **B196**, 189 (1982); See also D. D. Dietrich and F. Sannino, Phys. Rev. D **75**, 085018 (2007), for extensive investigation of the conformal window including nonfundamental representation fermions.
[11] Y. Iwasaki *et al.*, Phys. Rev. Lett. **69**, 21 (1992); Phys. Rev. D **69**, 014507 (2004); P. Damgaard, U. Heller, A. Krasnitz, and P. Olesen, Phys. Lett. B **400**, 169 (1997); R. Mawhinney, Nucl. Phys. B, Proc. Suppl. **83**, 57 (2000), for pioneering lattice studies on the phase structure of the large flavor gauge theories.
[12] S. Catterall and F. Sannino, Phys. Rev. D **76**, 034504 (2007).
[13] T. Appelquist, G. T. Fleming, and E. T. Neil, Phys. Rev. Lett. **100**, 171607 (2008).
[14] L. Del Debbio, A. Patella, and C. Pica, arXiv:0812.0570.
[15] L. Del Debbio, A. Patella, and C. Pica, arXiv:0805.2058.
[16] L. Del Debbio, M. T. Frandsen, H. Panagopoulos, and F. Sannino, J. High Energy Phys. 06 (2008) 007.
[17] S. Catterall, J. Giedt, F. Sannino, and J. Schneible, J. High Energy Phys. 11 (2008) 009.
[18] T. DeGrand, Y. Shamir, and B. Svetitsky, Phys. Rev. D **79**, 034501 (2009).
[19] Y. Shamir, B. Svetitsky, and T. DeGrand, Phys. Rev. D **78**, 031502 (2008).
[20] Z. Fodor *et al.*, arXiv:0809.4888.
[21] Z. Fodor *et al.*, arXiv:0809.4890.
[22] A. J. Hietanen, J. Rantaharju, K. Rummukainen, and K. Tuominen, J. High Energy Phys. 05 (2009) 025.
[23] T. Appelquist, G. T. Fleming, and E. T. Neil, Phys. Rev. D **79**, 076010 (2009).
[24] G. T. Fleming, Proc. Sci., LAT2008 (2008) 021.
[25] M. Luscher, P. Weisz, and U. Wolff, Nucl. Phys. **B359**, 221 (1991).
[26] G. de Divitiis *et al.*, Nucl. Phys. **B437**, 447 (1995).
[27] G. M. de Divitiis, R. Frezzotti, M. Guagnelli, and R. Petronzio, Nucl. Phys. **B433**, 390 (1995).
[28] G. M. de Divitiis, R. Frezzotti, M. Guagnelli, and R. Petronzio, Nucl. Phys. **B422**, 382 (1994).
[29] A. Coste, A. Gonzalez-Arroyo, J. Jurkiewicz, and C. P. Korthals Altes, Nucl. Phys. **B262**, 67 (1985).
[30] S. Chowla and A. Selberg, Proc. Natl. Acad. Sci. U.S.A. **35**, 371 (1949).
[31] E. Bilgici, A. Flachi, E. Itou, M. Kurachi, C.-J. D. Lin, H. Matsufuru, H. Ohki, T. Onogi, and T. Yamazaki (work in progress).
[32] E. Bilgici *et al.*, arXiv:0808.2875.
[33] S. Necco and R. Sommer, Nucl. Phys. **B622**, 328 (2002).
[34] E. Elizalde, Commun. Math. Phys. **198**, 83 (1998).
[35] K. Kirsten, J. Math. Phys. (N.Y.) **35**, 459 (1994).
[36] I. S. Gradshteyn and I. M. Ryzhik, *Tables of Integrals, Series, and Products* edited by A. Jeffrey and D. Zwillinger (Academic Press, New York, 2000), 6th ed.
[37] M. Luscher, R. Narayanan, P. Weisz, and U. Wolff, Nucl. Phys. **B384**, 168 (1992).
[38] S. Caracciolo *et al.*, Phys. Rev. Lett. **74**, 2969 (1995).
[39] M. Albanese *et al.*, Phys. Lett. B **192**, 163 (1987).
[40] S. Capitani, M. Luscher, R. Sommer, and H. Wittig, Nucl. Phys. **B544**, 669 (1999).
[41] M. Della Morte *et al.*, Nucl. Phys. **B713**, 378 (2005).
[42] M. Guagnelli, R. Sommer, and H. Wittig, Nucl. Phys. **B535**, 389 (1998).
[43] G. T. Fleming, arXiv:hep-lat/0403023.